COMPARISON BETWEEN PASSIVE AND ACTIVE FLEXIBLE ANTI-ROLL BARS MODELLED BY FINITE ELEMENT METHOD ON PREVENTION OF VEHICLE ROLLOVERS

Joed Henrique Paes*, Diego Colón*

*Av. Prof. Luciano Gualberto, travessa 3, n 158, CEP 05508-900
USP / Escola Politécnica - Laboratório de Automação e Controle (LAC)
São Paulo, São Paulo, Brazil

Emails: joedpaes@gmail.com, diego@lac.usp.br

Abstract— Anti-roll bars aims to increase the driving comfort by reducing the roll angle during cornering and also assist the self-steering behaviour of the vehicle chassis. This paper presents a comparison between a passive anti-roll bar and an active anti-roll bar. The bars are modelled by FEM (Finite Element Method) and a controller LQG (Linear Quadratic Gaussian) is designed to the active system. In addition, the vehicle lateral dynamic is hybridized to the flexible model in order to obtain an unique mathematical model. It reviews the vehicle roll dynamics and describes the FEM applied to dynamic modelling of flexible structures. The influence of the active anti-roll system is illustrated through numerical simulation, and a comparison among the passive anti-roll system and the system without anti-roll is also presented. To the best of the authors' knowledge, the modelling approach presented in Sections 3.1 and 3.2 have not been reported in the literature.

Keywords— Anti-roll system, flexible structures, control, finite element method.

Resumo— Barras de anti-rolagem visam aumentar o conforto através da redução do ângulo de rolagem em curvas e também auxiliam na auto-dirigibilidade do chassis do veículo. Este trabalho apresenta uma comparação entre um sistema com barra de anti-rolagem passiva e outro com barra. As barras são modeladas pelo MEF (Método dos Elementos Finitos) e um controlador LQG (Linear Quadrático Gaussiano) é projetado para o sistema ativo. Além disso, à dinâmica lateral do veículo, é adicionada a parte flexível para obter um único modelo matemático. O trabalho revisa a dinâmica de rolagem veícular e descreve o MEF aplicado à modelagem dinâmica de estruturas flexíveis. A influência do sistema ativo é ilustrada através de simulação, e uma comparação entre os sistemas passivo e sem barra de anti-rolagem também é apresentada. Até onde vai o conhecimento dos autores, a abordagem dada à modelagem nas Seções 3.1 e 3.2 não foi relatada na literatura.

Palavras-chave— Sistema anti-rolagem, estruturas flexíveis, controle, método dos elementos finitos.

Nomenclature

- l lateral distance between left and right suspensions.
- h height of the vehicle's c.g..
- a_y lateral acceleration of the vehicle.
- m_s vehicle sprung mass.
- m_u unsprung mass on vehicle's left/right side.
- I_{xx} roll moment of inertia about the c.g..
- g acceleration due to gravity.
- F_{lat} total lateral tire force.
- ϕ roll angle.
- z_s vertical deflection of the vehicle's c.g..
- z_{ul} vertical deflection of the left unsprung mass.
- z_{ur} vertical deflection of the right unsprung mass.
- z_{rl} left road displacement input.
- z_{rr} right road displacement input.
- k_s suspension stiffness.
- b_s suspension damping coefficient.
- k_t tire stiffness.
- v nodal displacements.
- EI bending rigidity.
- ρ mass density per unit length.
- $\dot{()}$ time derivative.
- $()^n$ n-order spacial derivative.

1 Introduction

The composition of the current automotive fleet consists of 36% of light trucks, minivans and sport utility vehicles (SUVs). Unfortunately, the rate of fatal rollovers for pickups is twice the rate for passenger cars, and the rate for SUVs is almost three times the rate for passenger cars. While rollover affects about 31% of passenger cars involved in crashes with occupant fatalities, it accounts for 51% of passenger cars occupant fatalities in single crashes. These statistics are from 2016 and has motivated several studies to improve passenger cars' safety by preventing rollover via active stability control (NHTSA, 2016).

An active anti-roll system allows the control of the roll angle and, thus, improves the vehicle stability, especially when turning or moving on slopping ground (Jamil et al., 2017). A rollover is a type of vehicle crash in which a vehicle tips over onto its side or roof and have a higher fatality rate than other types of vehicle collisions (Phanomchoeng and Rajamani, 2012).

This present paper is focused on finding hybridized dynamic models that merge the car's dynamic roll movement with a flexible anti-roll bar that is attached to the suspension system. This anti-roll bar can be passive or active. This last model must be well suited to the design of active feedback controllers, which are used to mitigate the rollover occurrence. Only linear time invariant models are considered. The flexible bar's mathematical model is obtained by FEM.

The suitability for controller synthesis is determined by a number of factors, including the accuracy of the model for moderate steering inputs (e.g. linear tire behaviour and small roll angles) and the order and simplicity of the dynamic model. The finite element approach produces models with large number of degrees of freedom, which causes numerical difficulties in dynamic analysis and control design. Thus, a model reduction is applied aiming to glean a suitable system with lower order to design the LQG controller.

The remainder of the paper is organized as follows: the section 2 presents the results of the literature survey. The section 3 presents the models chosen for this study. The control design is presented in the section 4. The section 5 exhibits the results taken from three models: 1) the roll dynamics model without anti-roll system, 2) with passive and 3) active anti-roll bar system as well. Finally, the section 6 presents preliminary conclusions from this ongoing study.

2 Literature survey

Carlson and Gerdes use Model Predictive Control (MPC) theory to develop a framework for automotive stability control. The framework is then demonstrated with a roll mode controller, which seeks to actively limit the peak roll angle of the vehicle while simultaneously tracking the driver's yaw rate command (Carlson and Gerdes, 2003).

Cameron and Brennan present results of an initial investigation into models and control strategies suitable to prevent vehicle rollover due to untripped driving maneuvers. A challenging task is identifying suitable vehicle's models from the literature, comparing these models with experimental results, and determining suitable parameters for the models (Cameron and Brennan, 2005).

A pair of MPC capable of modifying the nominal roll dynamics of a vehicle through control of the planar vehicle dynamics are presented by Beal and Gerdes. Each of these controllers is based on a linear model of the vehicle. Results from a nonlinear vehicle model demonstrate that the differential-drive technique results in significant lateral-longitudinal tire force coupling and saturation, which degrades the validity of the model used for controller design (Beal and Gerdes, 2010).

Kim presents the design of an active roll controller for a vehicle, as well as an experimental study using the electrically actuated roll control system. Firstly, parameter sensitivity analysis is performed based on the 3DOF linear vehicle model. The controller is designed in the framework of lateral acceleration control and gain-scheduled control scheme considering the varying parameters induced by laden and running vehicle condition (Kim and Park, 2004).

A method for designing a controller which uses an active anti-roll bar (AARB) and an electronic stability program (ESP) for rollover prevention is presented by Yim. An ESP can carry out active braking to reduce vehicle's speed and lateral acceleration to prevent rollover. The controller for the AARB was designed based on linear quadratic static output feedback control methodology, which attenuates the effect of lateral acceleration on the roll angle and the roll rate, by controling the suspension stroke and the tire's deflection of the vehicle (Yim et al., 2012).

3 Mathematical models

Assuming that the axles and tires have a known mass, a four degrees-of-freedom (dof) roll dynamic model is developed in the following, considering vertical translation of the sprung mass, denoted by z_s, vertical translation of the left unsprung mass, denoted by z_{ul}, vertical translation of the right unsprung mass, denoted by z_{ur}, as well as the roll motion of the sprung mass, denoted by ϕ. The Fig. 1 illustrates the modelled system.

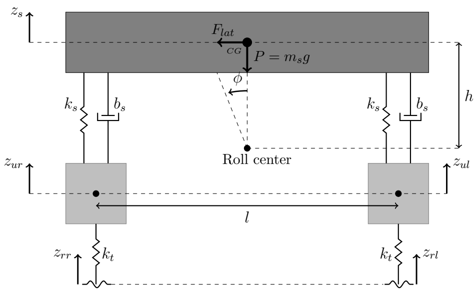

Figure 1: Four degree-of-freedom roll dynamics model (source: the authors).

Rajamani (Rajamani, 2012) shows that the overall equations of motion for the model is given by:

$$\begin{aligned} m_s \ddot{z}_s = & - k_s \left(2z_s - z_{ur} - z_{ul}\right) \\ & - b_s \left(2\dot{z}_s - \dot{z}_{ur} - \dot{z}_{ul}\right), \end{aligned} \tag{1}$$

$$\begin{aligned} m_{ur} \ddot{z}_{ur} = & \, k_s \left(z_s - \frac{l}{2} \sin\phi - z_{ur} \right) \\ & + b_s \left(\dot{z}_s - \frac{l}{2} \dot{\phi} \cos\phi - \dot{z}_{ur} \right) - k_t \left(z_{ur} - z_{rr} \right), \end{aligned} \tag{2}$$

$$m_{ul}\ddot{z}_{ul} = k_s\left(z_s + \frac{l}{2}\sin\phi - z_{ul}\right) + b_s\left(\dot{z}_s + \frac{l}{2}\dot{\phi}\cos\phi - \dot{z}_{ul}\right) - k_t\left(z_{ul} - z_{rl}\right), \tag{3}$$

and

$$\begin{aligned} J_s\ddot{\phi} =& m_s a_y h\cos\phi + m_s g h\sin\phi \\ &- \frac{k_s l^2}{2}\sin\phi - \frac{b_s l^2}{2}\dot{\phi}\cos\phi \\ &+ \frac{k_s l}{2}\left(z_{ul} - z_{ur}\right) + \frac{b_s l}{2}\left(\dot{z}_{ul} - \dot{z}_{ur}\right), \end{aligned} \tag{4}$$

where $J_s = (I_{xx} + m_s h^2)$.

3.1 Passive anti-roll bar

Consider a system, as shown in Fig. 2, which consists of a flexible bar connected to the unsprung masses of the roll dynamic model. It is desired to obtain a set of equations that represents this system so that the influence of the added bar show that the roll angle is reduced by this passive system when compared to the roll dynamic model. If EI is the equivalent bending rigidity, ρ is the mass density of the beam (per unit length) and $y(x,t)$ the deflection of the bar, the kinetic energy T and the potential energy V formulas are:

$$\begin{aligned} T =& \frac{m_s\dot{z}_s^2}{2} + \frac{m_{ur}\dot{y}^2(0,t)}{2} + \frac{m_{ul}\dot{y}^2(L,t)}{2} \\ &+ \frac{J_s\dot{\phi}^2}{2} + \frac{1}{2}\int_0^L \rho\dot{y}^2(x,t)\,\mathrm{d}x, \end{aligned} \tag{5}$$

$$\begin{aligned} V =& m_s g h\cos\phi + \frac{k_t}{2}\left(y(0,t) - z_{rr}\right)^2 \\ &+ \frac{k_t}{2}\left(y(L,t) - z_{rl}\right)^2 \\ &+ \frac{k_s}{2}\left(z_s - \frac{l}{2}\sin\phi - y(0,t)\right)^2 \\ &+ \frac{k_s}{2}\left(z_s + \frac{l}{2}\sin\phi - y(L,t)\right)^2 \\ &+ \frac{1}{2}\int_0^L EI\left(y''(x,t)\right)^2\,\mathrm{d}x. \end{aligned} \tag{6}$$

The Lagrangian's formula is:

$$L = T - V = L_D + \int_0^L \hat{L}\,\mathrm{d}x + L_B, \tag{7}$$

where $\hat{L}$ is a Lagrangian density and in which:

$$\begin{aligned} L_D =& \frac{J_s\dot{\phi}^2}{2} + \frac{m_s\dot{z}_s^2}{2} - m_s g h\cos\phi \\ &- k_s z_s^2 - k_s\frac{l^2}{4}\sin^2\phi, \end{aligned} \tag{8}$$

and

$$\hat{L} = \frac{1}{2}\rho\dot{y}^2(x,t) - \frac{1}{2}EI\left(y''(x,t)\right)^2, \tag{9}$$

and

$$\begin{aligned} L_B =& \frac{m_{ur}\dot{y}^2(0,t)}{2} + \frac{m_{ul}\dot{y}^2(L,t)}{2} - \frac{k_t}{2}\left(y(0,t) - z_{rr}\right)^2 \\ &- \frac{k_t}{2}\left(y(L,t) - z_{rl}\right)^2 - \frac{k_s y^2(0,t)}{2} - \frac{k_s y^2(L,t)}{2} \\ &- \frac{k_s}{2} l\sin\phi\left(y(0,t) - y(L,t)\right) \\ &+ k_s z_s\left(y(0,t) + y(L,t)\right). \end{aligned} \tag{10}$$

The generalized Hamilton's principle is used to derive the equations of motion, i.e.:

$$\int_{t_0}^{t_f}\left[\delta L_B + \int_0^L \delta\hat{L}\,\mathrm{d}x + \delta L_B + \delta W_{nc}\right]\,\mathrm{d}t = 0, \tag{11}$$

where the virtual works of a dissipative force and external forces are given by:

$$\begin{aligned} \delta W_{nc} =& \Bigg[F_{lat}h\cos\phi - b_s\frac{l^2}{2}\dot{\phi}\cos^2\phi) \\ &+ b_s\frac{l}{2}\cos\phi\big(\dot{y}(L,t) - \dot{y}(0,t)\big)\Bigg]\delta\phi \\ &+ \left[b_s\left(\dot{y}(0,t) + \dot{y}(L,t)\right) - 2b_s\dot{z}_s\right]\delta z_s \\ &+ \left[b_s\left(\dot{z}_s - \frac{l}{2}\dot{\phi}\cos\phi - \dot{y}(0,t)\right)\right]\delta y(0,t) \\ &+ \left[b_s\left(\dot{z}_s + \frac{l}{2}\dot{\phi}\cos\phi - \dot{y}(L,t)\right)\right]\delta y(L,t). \end{aligned} \tag{12}$$

The discretization techniques, such as finite differences, finite elements, and the Rayleigh-Ritz method, are appropriate to extract the characteristics of the systems. In this paper, the finite element method is applied, which is based on selection of a set of shape functions satisfying the geometric boundary conditions of the problem. We will search for solutions of the form:

$$y(x,t) = \sum_{i=1}^{n} N_i(x)v_i(t), \tag{13}$$

where n is the number of degree of freedom of the element, $N(x)$ are known polynomial shape functions of the spatial coordinates, which are linearly independent over the domain $0 \leq x \leq L$ as expressed in Eq. 14, and $v(t)$ are unknown functions of the time t:

$$N_i(x) = C_{1i} + C_{2i}x + C_{3i}x^2 + ..., i = 1, ..., n. \tag{14}$$

Hence the variations of the displacements can be put in a matrix form as in Eq. 15.

$$\delta y = N\delta v. \tag{15}$$

The substitution of Eq. 15 into the variational principle in Eq. 11 leads to:

$$m\ddot{v} + c\dot{v} + kv = fd, \tag{16}$$

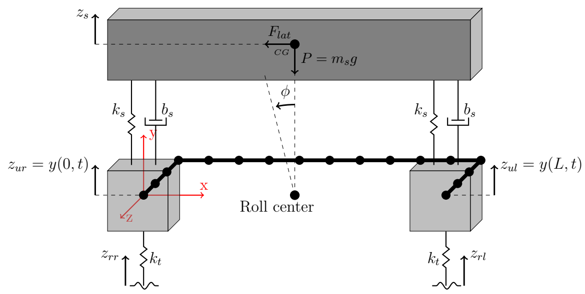

Figure 2: Roll dynamic model with passive anti-roll bar (source: the authors).

where:

$$m = \begin{bmatrix} J_s & 0 & 0 \\ 0 & m_s & 0 \\ 0 & 0 & m_{22} \end{bmatrix}, \tag{17}$$

$$c = \begin{bmatrix} b_s \frac{l^2}{2} & 0 & b_s \frac{l}{2}\left(N(0) - N(L)\right) \\ 0 & 2b_s & -b_s\left(N(0) + N(L)\right) \\ b_s \frac{l}{2}\left(N^T(0) - N^T(L)\right) & -b_s\left(N^T(0) + N^T(L)\right) & b_s\left(N^T(0)N(0) + N^T(L)N^T(L)\right) \end{bmatrix}, \tag{18}$$

$$k = \begin{bmatrix} k_s \frac{l^2}{2} - m_s gh & 0 & k_s \frac{l}{2}\left(N(0) - N(L)\right) \\ 0 & 2k_s & -k_s\left(N(0) + N(L)\right) \\ k_s \frac{l}{2}\left(N^T(0) - N^T(L)\right) & -k_s\left(N^T(0) + N^T(L)\right) & k_{22} \end{bmatrix}, \tag{19}$$

$$f = \begin{bmatrix} m_s h & 0 & 0 \\ 0 & 0 & 0 \\ 0 & k_t N^T(0) & k_t N^T(L) \end{bmatrix}, \tag{20}$$

where

$$\begin{aligned} m_{22} = M_v &+ N^T(0) m_{ur} N(0) \\ &+ N^T(L) m_{ul} N(L), \end{aligned} \tag{21}$$

$$\begin{aligned} k_{22} = K_v &+ N^T(0)\left(k_s + k_t\right) N(0) \\ &+ N^T(L)\left(k_s + k_t\right) N(L), \end{aligned} \tag{22}$$

$$M_v = \int_0^L \rho N^T(x) N(x)\, \mathrm{d}x, \tag{23}$$

$$K_v = \int_0^L EI N''^T(x) N''(x)\, \mathrm{d}x, \tag{24}$$

and

$$\begin{aligned} v &= \left(\phi, z_s, v_1, v_2, ..., v_n\right)^T, \\ d &= \left(a_y, z_{rr}, z_{rl}\right)^T. \end{aligned} \tag{25}$$

3.2 Active anti-roll bar

Consider the system, as shown in Fig. 3, which consists of two flexible bars, each one connected to an unsprung mass and the electric motor, which provides the control torque for the active system. As in the previous section, it is desired to seek a set of equations that represents the system, so that the influence of the control torque shows that the roll angle will be minimized by the active system when compared to the passive system. Denote by $y_A(x,t)$ the deflection of the bar A and $y_B(x,t)$ the deflection of the bar B. The kinetic energy T and potential energy V expressions are:

$$\begin{aligned} T =& \frac{m_s \dot{z}_s^2}{2} + \frac{m_{ur} \dot{y}_A^2(0,t)}{2} + \frac{m_{ul} \dot{y}_B^2(L,t)}{2} + \frac{J_s \dot{\phi}^2}{2} \\ &+ \frac{1}{2}\int_0^L \rho \dot{y}_A^2(x,t)\, \mathrm{d}x + \frac{1}{2}\int_0^L \rho \dot{y}_B^2(x,t)\, \mathrm{d}x, \end{aligned} \tag{26}$$

$$\begin{aligned} V =& m_s gh\cos\phi + \frac{k_t}{2}\left(y_A(0,t) - z_{rr}\right)^2 \\ &+ \frac{k_t}{2}\left(y_B(L,t) - z_{rl}\right)^2 \\ &+ \frac{k_s}{2}\left(z_s - \frac{l}{2}\sin\phi - y_A(0,t)\right)^2 \\ &+ \frac{k_s}{2}\left(z_s + \frac{l}{2}\sin\phi - y_B(L,t)\right)^2 \\ &+ \frac{1}{2}EI\int_0^L \left(\left(y_A''(x,t)\right)^2 + \left(y_B''(x,t)\right)^2\right)\, \mathrm{d}x. \end{aligned} \tag{27}$$

As in Eq. 7, the Lagrangian terms are:

$$\begin{aligned} L_D =& \frac{J_s \dot{\phi}^2}{2} + \frac{m_s \dot{z}_s^2}{2} - m_s gh\cos\phi \\ &- k_s z_s^2 - k_s \frac{l^2}{4}\sin^2\phi, \end{aligned} \tag{28}$$

$$\begin{aligned} \hat{L} =& \frac{1}{2}\rho \dot{y}_A^2(x,t) + \frac{1}{2}\rho \dot{y}_B^2(x,t) \\ &- \frac{1}{2}EI\left(y_A''(x,t)\right)^2 - \frac{1}{2}EI\left(y_B''(x,t)\right)^2, \end{aligned} \tag{29}$$

$$\begin{aligned} L_B =& \frac{m_{ur} \dot{y}_A^2(0,t)}{2} + \frac{m_{ul} \dot{y}_B^2(L,t)}{2} \\ &- \frac{k_t}{2}\left(y_A(0,t) - z_{rr}\right)^2 - \frac{k_t}{2}\left(y_B(L,t) - z_{rl}\right)^2 \\ &- \frac{k_s y_A^2(0,t)}{2} - \frac{k_s y_B^2(L,t)}{2} \\ &- k_s \frac{l}{2}\sin\phi\left(y_A(0,t) - y_B(L,t)\right) \\ &+ k_s z_s\left(y_A(0,t) + y_B(L,t)\right). \end{aligned} \tag{30}$$

Again, the generalized Hamilton's principle (Eq. 11) is used to derive the equations of motion, where the virtual work of dissipative and external forces, considering the control torque provided by the motor, is given by:

$$\begin{aligned} \delta W_{nc} =& \Big[F_{lat} h\cos\phi + b_s \frac{l}{2}\cos\phi\left(\dot{y}_B(L,t) - \dot{y}_A(0,t)\right) \\ &- b_s \frac{l^2}{2}\dot{\phi}\cos^2\phi)\Big]\delta\phi - u\delta\theta_{y_A(L,t)} + u\delta\theta_{y_B(0,t)} \\ &+ \left[b_s\left(\dot{y}_A(0,t) + \dot{y}_B(L,t)\right) - 2b_s \dot{z}_s\right]\delta z_s \\ &+ \left[b_s\left(\dot{z}_s - \frac{l}{2}\dot{\phi}\cos\phi - \dot{y}_A(0,t)\right)\right]\delta y_A(0,t) \\ &+ \left[b_s\left(\dot{z}_s + \frac{l}{2}\dot{\phi}\cos\phi - \dot{y}_B(L,t)\right)\right]\delta y_B(L,t), \end{aligned} \tag{31}$$

where u is the torque input applied by the motor. As a simplification, the dynamic model of the motor is neglected and the torque is directly applied as moments at the tips of each bar connected to the motor, as shown in Fig. 3.

Likewise the previous section, the finite element method is employed in this analysis, where:

$$y_k(x,t) = \sum_{i=1}^{n} N_{ki}(x) v_{ki}(t), \tag{32}$$

and $k = A, B$. Hence the variations of the displacements have the form:

$$\delta y_k = N_k \delta v_k. \tag{33}$$

The substitution of Eq. 33 for each bars into the variational principle in Eq. 11 leads to:

$$m\ddot{v} + c\dot{v} + kv = fd + hu, \tag{34}$$

where:

$$m = \begin{bmatrix} J_s & 0 & 0 & 0 \\ 0 & m_s & 0 & 0 \\ 0 & 0 & m_{22} & 0 \\ 0 & 0 & 0 & m_{33} \end{bmatrix}, \tag{35}$$

$$c = \begin{bmatrix} b_s \frac{l^2}{2} & 0 & b_s \frac{l}{2} N_A(0) & -b_s \frac{l}{2} N_B(L) \\ 0 & 2b_s & -b_s N_A(0) & -b_s N_B(L) \\ b_s \frac{l}{2} N_A^T(0) & -b_s N_A^T(0) & b_s N_A^T(0) N_A(0) & 0 \\ -b_s \frac{l}{2} N_B^T(L) & -b_s N_B^T(L) & 0 & b_s N_B^T(L) N_B(L) \end{bmatrix}, \tag{36}$$

$$k = \begin{bmatrix} k_s \frac{l^2}{2} - m_s g h & 0 & k_s \frac{l}{2} N_A(0) & -k_s \frac{l}{2} N_B(L) \\ 0 & 2k_s & -k_s N_A(0) & -k_s N_B(L) \\ k_s \frac{l}{2} N_A^T(0) & -k_s N_A^T(L) & k_{22} & 0 \\ -k_s \frac{l}{2} N_B^T(L) & -k_s N_B^T(L) & 0 & k_{33} \end{bmatrix}, \tag{37}$$

$$f = \begin{bmatrix} m_s h & 0 & 0 \\ 0 & 0 & 0 \\ 0 & k_t N_A^T(0) & 0 \\ 0 & 0 & k_t N_B^T(L) \end{bmatrix}, \tag{38}$$

$$h = \begin{bmatrix} 0 \\ 0 \\ -N_A^T(L) \\ N_B^T(0) \end{bmatrix}, \tag{39}$$

where:

$$m_{22} = M_{v_A} + m_{ur} N_A^T(0) N_A(0), \tag{40}$$

$$m_{33} = M_{v_B} + m_{ul} N_B^T(L) N_B(L), \tag{41}$$

$$k_{22} = K_{v_A} + (k_s + k_t) N_A^T(0) N_A(0), \tag{42}$$

$$k_{33} = K_{v_B} + (k_s + k_t) N_B^T(L) N_B(L), \tag{43}$$

$$M_{vi} = \int_0^L \rho N_i^T(x) N_i(x) \, \mathrm{d}x, \tag{44}$$

$$K_{vi} = \int_0^L EI N_i''^T(x) N_i''(x) \, \mathrm{d}x, \tag{45}$$

and

$$\begin{aligned} v &= (\phi, z_s, v_{A_1}, v_{A_2}, ..., v_{A_n}, v_{B_1}, v_{B_2}, ..., v_{B_n})^T, \\ d &= (a_y, z_{rr}, z_{rl})^T. \end{aligned} \tag{46}$$

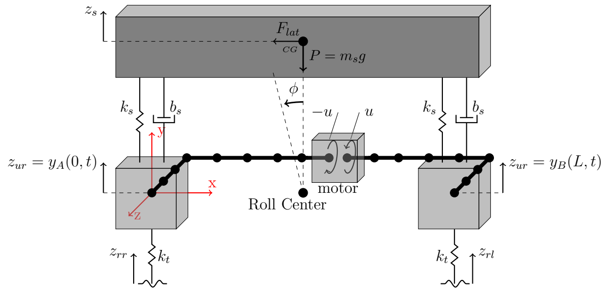

Figure 3: Roll dynamic model with active anti-roll bar (source: the authors).

3.3 Parameters

Table 1 presents the parameter's values used for simulation. These parameters were obtained by Yim from an small SUV car in software CarSim®(Yim et al., 2012).

Table 1: Parameters values.

Variable	Value	Units
m_s	984.6/2	kg
m_{ur}	40	kg
m_{ul}	40	kg
h	0.45	m
I_{xx}	439.9/2	kgm^2
k_s	28721	N/m
b_s	2000	$n/(m/s)$
k_t	230000	N/m
l	1.6	m
g	9.81	m/s^2
E	210	GPa
ρ	7850	kg/m^3

Table 2: Passive bar geometry coordinates.

Spatial distribution of the nodes			
Description	x [m]	y [m]	z [m]
n_1	0	0	0
n_2	0	0	-0.1
n_3	0	0	-0.2
n_4	0	0	-0.3
n_5	0.2	0	-0.3
n_6	0.4	0	-0.3
n_7	0.6	0	-0.3
n_8	0.8	0	-0.3
n_9	1.0	0	-0.3
n_{10}	1.2	0	-0.3
n_{11}	1.4	0	-0.3
n_{12}	1.6	0	-0.3
n_{13}	1.6	0	-0.2
n_{14}	1.6	0	-0.1
n_{15}	1.6	0	0

Figure 4 illustrates the spatial discretization of the passive bar. Table 2 shows the coordinates xyz of each node. All models use beam element, where each node has six dof's: displacements xyz and their respective rotations. The cross-section is circular with radius $r = 21.8mm$.

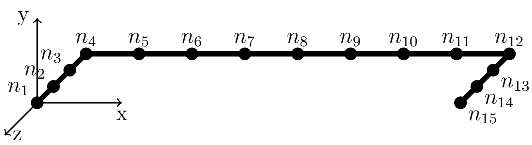

Figure 4: Geometry of the passive bar (source: the authors).

Figure 5 illustrates the spatial discretization of the active bar. The Tables 3 and 4 shows the coordinates x-y-z of each node.

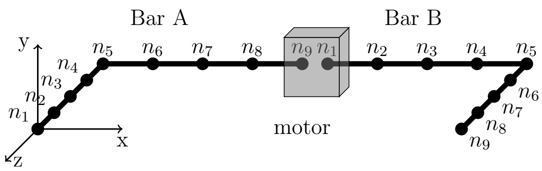

Figure 5: Geometry of the active anti-roll bar (source: the authors).

Table 3: Active bar "A" geometric coordinates.

Spatial distribution of the nodes			
Description	x	y	z
n_1	0	0	0
n_2	0	0	-0.1
n_3	0	0	-0.2
n_4	0	0	-0.3
n_5	0.2	0	-0.3
n_6	0.4	0	-0.3
n_7	0.6	0	-0.3
n_8	0.8	0	-0.3

Table 4: Active bar "B" geometric coordinates.

Spatial distribution of the nodes			
Description	x	y	z
n_1	0.8	0	-0.3
n_2	1.0	0	-0.3
n_3	1.2	0	-0.3
n_4	1.4	0	-0.3
n_5	1.6	0	-0.3
n_6	1.6	0	-0.2
n_7	1.6	0	-0.1
n_8	1.6	0	0

4 Control design

The design of LQG control law for the active anti-roll system is performed in two steps, where the model is expressed in following form:

$$\begin{aligned} \dot{x} &= Ax + Bu + Gw, \\ y &= Cx + v, \end{aligned} \tag{47}$$

where w is white process noise signal and v is the white measurement noise signal.

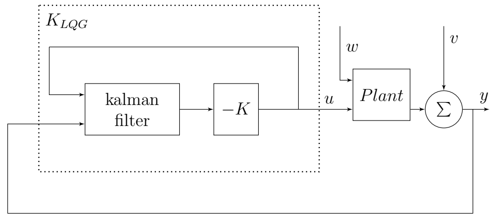

Figure 6: LQG scheme (source: the authors).

Considering Fig. 6: the Kalman filter is firstly determined by minimizing the steady-state error covariance $E[e(t), e^T(t)]$, where the error is $e(t) = x(t) - \hat{x}(t)$. The process of minimization of the error covariance is strongly associated with the matrices Ξ and Θ, that are expressed in Eq. 48, which also represent the covariances of the process and measurement noises, respectively:

$$E[ww^T] = \Xi, \quad E[vv^T] = \Theta, \quad E[wv^T] = \Psi. \tag{48}$$

Properly chosen values of the above matrices lead to the gain L of Kalman filter, that is:

$$\dot{\hat{x}} = A\hat{x} + Bu + L[y - C\hat{x}]. \tag{49}$$

The state feedback gain matrix K is determined by the minimization of the cost functional expressed in Eq. 50 for the particular selection of the weight matrices Q and R:

$$J = \frac{1}{2}\int_0^\infty \left(x^T Q x + u^T R u\right) \, \mathrm{d}t. \tag{50}$$

The control law resulting from this process has the following form:

$$u = -K\hat{x}, \tag{51}$$

where $\hat{x}$ is the estimated values delivered by the Kalman filter.

Finally, the state-space equation of LQG controller with the Kalman filter can be written in following form:

$$\begin{aligned} \dot{\hat{x}} &= [A - LC - BK]\,\hat{x} + Ly, \\ u &= -K\hat{x}, \end{aligned} \tag{52}$$

where y is the vector of the plant's output (sensors) measurements.

5 Results

For the analysis, it was adopted a known unitary lateral acceleration input aiming to compare the final results between the three models chosen for simulation. The chosen input represents a moderate driver's maneuver that starts a cornering at 1.0 second and maintain a circular trajectory for 3.0 seconds. Figure 7 illustrates the lateral acceleration used as input to the models.

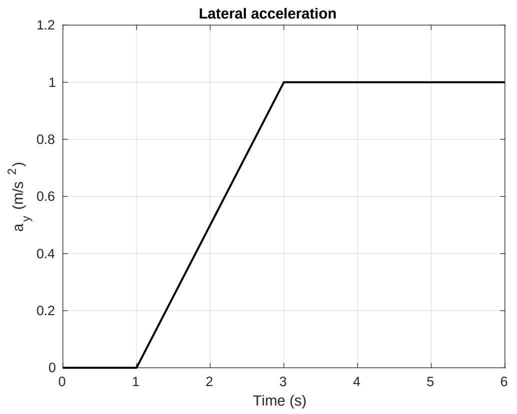

Figure 7: Input taken for lateral acceleration (source: the authors).

Typically, the models provided by the finite element method present large number of degree of freedom, and the design of the controller becomes a complicated task. In this paper, the order reduction through truncation was applied by using the Hankel singular values of the balanced representation of the system. Figure 8 shows the original model with 196 states and the reduced model with the four more relevant states to the controller design. The obtained controller was applied to the original system. In the first step, the gain L of the Kalman filter is determined. In this case, the steady-state error covariance is minimized by choosing the weighting matrices Q and R as:

$$Q = \left[C^T C\right], \quad R = \left[1e^{-12}\right]. \tag{53}$$

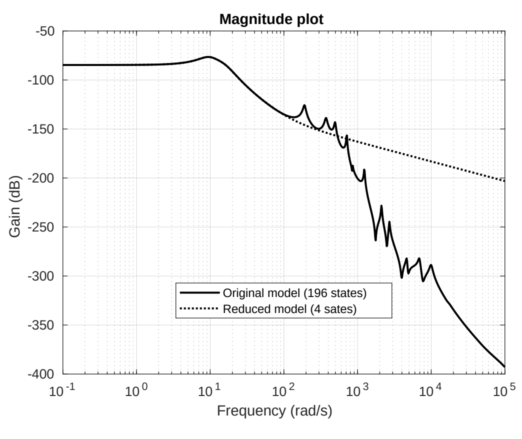

Figure 8: Magnitude plot of the original and reduced models for active anti-roll bar (source: the authors).

In order to improve steady-state response of controller, an integrator was added throughout the designing. The controller's transfer function obtained is given in Eq. 54, where $8e6$ stands for 8×10^6 and so forth:

$$K(s) = \frac{8e6s^4 + 1e8s^3 + 3e9s^2 + 2e10s + 1e11}{s^6 + 56s^5 + 2e3s^4 + 4e4s^3 + 5e5s^2 + 3e6s} \tag{54}$$

Figure 9 a) shows the model eigenvalues without anti-roll system, which is naturally stable with all complex conjugate poles. In Fig. 9 b) it is presented both passive and active anti-roll system poles. It is seen the typical characteristics of flexible structures, which are the complex conjugate poles with small real parts. The addition of the controller included some real poles with large real part in order to attain the control objective. Figure 9 c) shows a zoom of b) where it is seen the controller's influence in the poles near the origin. The arc pattern of the poles resulted of the application of the Rayleigh damping on the flexible portion to make the system well conditioned numerically.

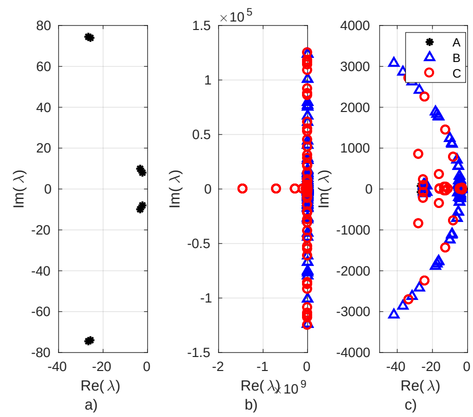

Figure 9: Eigenvalues for the systems: A(without anti-roll bar), B(passive bar), C(active bar) (source: the authors).

Figure 10 shows the main result of this work. The system without anti-roll bar suffers a roll angle of 0.58 degree under influence of a unitary lateral acceleration. When the passive bar is added, the roll angle is reduced to 0.41, that represents a decrease of approximately 30%. The passive bar also improves the roll occurrence during the ramp acceleration between 1.0 and 3.0 seconds. The third model, with active bar, reduces the roll angle to zero under influence of the unitary lateral acceleration at steady-state. During the ramp acceleration, the active model is not able to reduce the roll angle to zero. However, the controller tends to maintain the roll angle below 0.1 degree.

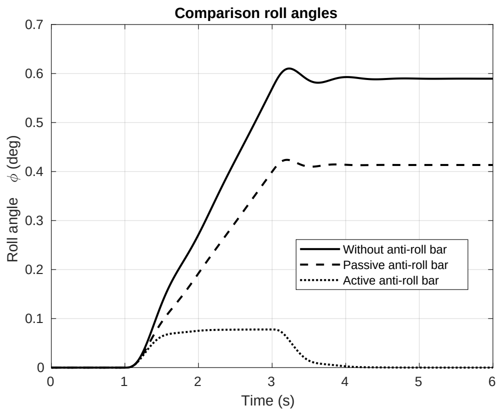

Figure 10: Roll angle for system: 1) without bar, 2) with passive and 3) with active anti-roll bar (source: the authors).

The active system presented a dc gain of $299Nm/degree$. It means that the motor provides $299Nm$ of torque to compensate one degree of roll angle. This value is similar to others presented in the literature, on real active anti-roll system (Bharane et al., 2014). Figure 11 shows the control torque applied by the motor whereby the roll angle was reduced. While the vehicle was cornering at a circular trajectory, the motor kept a torque of $122Nm$ to compensate the roll angle.

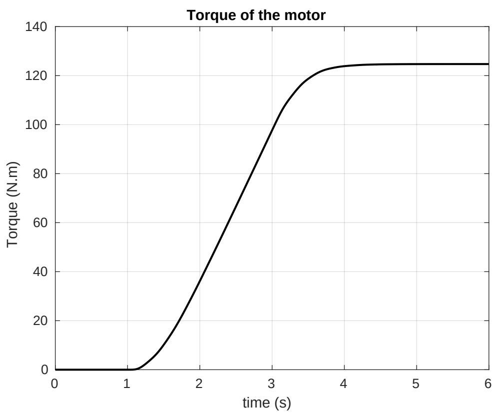

Figure 11: Control signal: torque provided by the motor (source: the authors).

6 Conclusion

There is a significant opportunity to improve the safety of the current fleet by preventing vehicle rollover. In this work, it was proposed a model of the flexible anti-roll bar system with FEM in both passive and active version. The model proposed was hybrid, in the sense that it integrated the lumped parameter part (roll vehicle's dynamic) and the flexible part. The active model was used to design a LQG controller to reduce the rolling. The passive anti-roll bar reduced the roll behaviour in 30% compared to the system without it. On the other hand, the active bar reduced the roll angle to zero under constant lateral acceleration and showed a significant reduction during varying lateral acceleration.

Acknowledgements

The authors would like to thank the reviewers for their thoughtful comments on the first draft of this paper.

References

Beal, C. E. and Gerdes, J. C. (2010). Predictive control of vehicle roll dynamics with rear wheel steering, *American Control Conference (ACC), 2010*, IEEE, pp. 1489–1494.

Bharane, P., Tanpure, K., Patil, A. and Kerkal, G. (2014). Design, analysis and optimization of anti-roll bar, *Journal of Engineering Research and Applications* **4**(9): 137–140.

Cameron, J. T. and Brennan, S. (2005). A comparative, experimental study of model suitability to describe vehicle rollover dynamics for control design, *ASME*, American Society of Mechanical Engineers, pp. 405–414.

Carlson, C. R. and Gerdes, J. C. (2003). Optimal rollover prevention with steer by wire and differential braking, *ASME*, American Society of Mechanical Engineers, pp. 345–354.

Jamil, F. M., Abdullah, M., Ibrahim, M., Harun, M. and Abdullah, W. W. (2017). The dynamic verification of vehicle roll dynamic models using different softwares, *Proceedings of Innovative Research and Industrial Dialogue* **16**: 135–136.

Kim, H.-J. and Park, Y.-P. (2004). Investigation of robust roll motion control considering varying speed and actuator dynamics, *Mechatronics* **14**(1): 35–54.

NHTSA (2016). Passenger vehicle occupant fatalities, https://www.nhtsa.gov/. Accessed: 2018-02-30.

Phanomchoeng, G. and Rajamani, R. (2012). Prediction and prevention of tripped rollovers.

Rajamani, R. (2012). *Vehicle Dynamics and Control*, Mechanical Engineering Series, 2 edn, Springer US.

Yim, S., Jeon, K. and Yi, K. (2012). An investigation into vehicle rollover prevention by coordinated control of active anti-roll bar and electronic stability program, *International Journal of Control, Automation and Systems* **10**(2): 275–287.